arXiv:1408.3970v1 [hep-ph] 18 Aug 2014

RS resonance in di-final state production at the LHC to NLO+PS accuracy

Goutam Das [a,1] , Prakash Mathews [a,2] , V. Ravindran [b,3] , Satyajit Seth [a,4]

[a] Saha Institute of Nuclear Physics,
1/AF Bidhan Nagar, Kolkata 700 064, India

[b]The Institute of Mathematical Sciences,
Tharamani, Chennai 600 113, India

Abstract

We study the di-final state processes ($\ell^+\ell^-$, $\gamma\gamma$, ZZ, W^+W^-) to NLO+PS accuracy, as a result of both the SM and RS Kaluza-Klein graviton excitations. Decay of the electroweak gauge boson final states to different leptonic states are included at the showering stage. A selection of the results has been presented with PDF and scale uncertainties for various distributions. Using the di-lepton and di-photon final states, we present the search sensitivity, for the 14 TeV LHC at 50 fb^{-1} luminosity.

[1]goutam.das@saha.ac.in
[2]prakash.mathews@saha.ac.in
[3]ravindra@imsc.res.in
[4]satyajit.seth@saha.ac.in

1 Introduction:

With the discovery of a new scalar particle at the Large Hadron Collider (LHC) and with the additional data on completion of Run I, it now appears that the scalar particle is more and more likely to be the Standard Model (SM) Higgs boson. At the LHC, there has been no evidence of new physics so far. Nonetheless we know that the SM on many counts is not a complete description of nature. The SM can account for only a meager 4% of the energy composition of the universe, does not account for the observed phenomena in the neutrino sector. Also the theoretical criterion of naturalness needs the presence of physics beyond the SM at the TeV scale. As the properties of the Higgs boson become known with greater precision, signs of new physics might show up. We are hence gearing up to the Run II with higher center of mass energies at the LHC.

Search of physics beyond the SM is an important objective of the LHC physics program and is motivated by the large hierarchy that exists between the gravitational Planck scale and the electroweak symmetry breaking scale. Among various options, an interesting alternative that addressed the hierarchy problem was achieved by invoking extra spacial dimensions in TeV scale brane world scenarios [1, 2, 3]. Classification based on the geometry of extra spacial dimension leads to two classes of model *viz.* the factorisable [1, 2] and non-factorisable extra dimensions [3]. In both these models the SM particles are constrained in the 4-dimensional world and only gravity is allowed in the extra dimensional bulk. The ADD model with factorisable extra dimensions, has negligible curvature results in a tower of spin-2 Kaluza-Klein (KK) modes while the RS model with non-factorisable extra dimension has significant curvature leading to narrow spin-2 KK mode resonances. The phenomenology of these two models are quite distinct, with the ADD model leading to an enhancement of the tale of the invariant mass distribution as a result of the combined effect of the tower of KK modes. In contrast, the RS model leads to the production of a narrow width RS KK mode resonances.

The geometry of the RS model consists of an extra spacial dimension ϕ which is warped, wherein two 3-branes are placed at orbifold fixed points at $\phi = 0$ (Planck brane) and $\phi = \pi$ (TeV brane). The SM particles are constrained on the TeV brane, while gravity originates on the Planck brane and are allowed to propagate in the bulk. The tower of KK excitations ($h^{(n)}_{\mu\nu}$) of the graviton couples to the SM energy momentum tensor ($T^{\mu\nu}$) through the following interaction Lagrangian [4],

$$\mathcal{L}_{int} \;=\; -\frac{1}{\overline{M_p}} T^{\mu\nu}(x) h^{(0)}_{\mu\nu}(x) - \frac{e^{\pi\mathcal{K}R_c}}{\overline{M_p}} \sum_{n=1}^{\infty} T^{\mu\nu}(x) h^{(n)}_{\mu\nu}(x) \qquad , \tag{1}$$

where $\overline{M_p}$ is the reduced Planck scale, $\mathcal{K}$ is the curvature assumed to be of the same order as M_p and R_c is the radius of compactification. The first term in the above Lagrangian denotes the contribution of the zero mode graviton which is M_p suppressed. However, due to the exponential warping the higher dimensional Planck

scale could be of the order of the electroweak scale. As a consequence, it is customary to neglect the zero mode of graviton excitation and consider the following interaction Lagrangian without any loss of generality,

$$\mathcal{L}_{int}^{\rm RS} = -\frac{\overline{c_0}}{m_0}\sum_{n=1}^{\infty} T^{\mu\nu}(x)h_{\mu\nu}^{(n)}(x) \qquad , \tag{2}$$

where $\overline{c_0} = \mathcal{K}/\overline{M_p}$ is an effective coupling and $m_0 = \mathcal{K}e^{-\pi\mathcal{K}R_c}$ sets a mass scale for the massive KK mode gravitons. The 5-dimensional metric is non-factorisable and this leads to a spectrum of KK modes whose masses are given by,

$$M_n = x_n\ \mathcal{K}\ e^{-\pi\mathcal{K}R_c} \qquad , \tag{3}$$

where x_ns' are the roots of the Bessel function $J_1(x)$. The RS model is characterised by the dimensionless coupling $\overline{c_0}$ and the first KK mode excitation mass M_1.

The KK modes could be produced *via* the $q\bar{q}$ channel or the gg channel which would then decay to SM bosons or fermions leading to di-final states. These processes are being explored at the LHC leading to bounds on the model parameters [5, 6, 7, 8]. Of course, to put stringent bounds on the model parameters at a hadron collider like the LHC, it is essential to have the next-to-leading order (NLO) QCD corrections, as the leading order (LO) predictions suffer from large theoretical uncertainties. Presently the di-final state processes are available to NLO accuracy for DY [9, 10], di-photon [11, 12], ZZ [13, 14], W^+W^- [15, 16] and di-jet [17] for the extra dimension scenarios ADD and RS. This has been further extended to the NLO+PS accuracy for the ADD model for the di-final state processes [18, 19], excluding the jets. As the K-factor at NLO level is large, attempts to go beyond NLO in QCD are underway and there are already first results [20, 21, 22] at NNLO level in the threshold limit for Drell-Yan production in gravity mediated models.

In this paper, we present the di-final state production processes (except those containing jet(s) in the LO) at hadron colliders which are interfaced with Parton Shower (PS) Monte Carlo to NLO accuracy using the MC@NLO formalism for the RS model. It should be pointed out that, the success to fully automatise the SM calculations to this accuracy is rather recent [23], but the status of BSM models to the same accuracy is still wanting. Precise theoretical predictions to NLO+PS accuracy are extremely desirable for the RS model and hence these codes are being made available for the LHC community. Various physical observables are studied, which are of relevance to future studies of these processes. These processes have been probed at the LHC Run I, in the SM, Higgs production and BSM searches and a more detailed study is expected in the Run II.

Rest of the paper is organised as follows: In section 2 we describe the NLO results for the di-final state processes and match them to parton shower Monte Carlo. The numerical results are presented in section 3 and finally we summarise our results in the last section.

2 NLO with PS

We have considered NLO QCD corrections to all the jet-exclusive tree level di-final state processes, namely Drell-Yan, di-photon, ZZ and W^+W^- production processes in the SM as well as in the RS scenario and these $\mathcal{O}(\alpha_s)$ corrected results are then matched with parton shower Monte Carlo using MC@NLO formalism [24]. The total RS contribution represents both the signal and background together consisting of pure SM, pure BSM and the interference between the two, whereas the SM contribution alone is treated as background.

For all the above mentioned processes, the parton level Born squared amplitude in the SM comes only from $q\bar{q}$ initiated Feynman diagrams, while in the RS model both $q\bar{q}$ and gg initiated Feynman diagrams contribute. In addition there is interference terms between the SM and RS model subprocesses. In the fixed order analysis, the $\mathcal{O}(\alpha_s)$ correction terms correspond to two categories of Feynman diagrams: (i) real emission and (ii) one-loop virtual correction. In the real emission part, $q\bar{q}$ or gg initiated subprocesses contribute leading to an extra gluon emission in addition to the desired final state. The $\bar{q}(q)g$ initiated partonic subprocesses begin to contribute at $\mathcal{O}(\alpha_s)$. Matrix elements coming from the one-loop virtual diagrams participate in the $\mathcal{O}(\alpha_s)$ correction, when multiplied by the corresponding Born amplitude. All these partonic subprocesses producing $\mathcal{O}(\alpha_s)$ correction terms behave alike for all of our processes of interest. Moreover, one additional $\mathcal{O}(\alpha_s)$ contribution shows up in the fixed order calculation for the di-boson final state processes due to the interference between gg initiated box diagrams in the SM and gg initiated Born diagrams in the RS scenario. We have taken care of all the aforesaid contributions in our present calculation.

While dealing with Drell-Yan process, we have only considered e^+e^- final state, as the other possible channel *i.e.* $PP \to \mu^+\mu^- X$ would be phenomenologically same with the chosen one, apart from the experimental identification of the final state particles.

In case of di-photon production, we have adopted smooth cone isolation technique [25] proposed by Frixione to get rid of using fragmentation contribution which are non-perturbative in nature which indicate the probability of fragmenting a parton into photon. We call it as Frixione isolation (FI) which ensures that soft radiation is not eliminated in any region of phase space and at the same time guarantees infra-red (IR) safety of the observable. In order to implement it, a cone of radius $r = \sqrt{(\eta - \eta_\gamma)^2 + (\phi - \phi_\gamma)^2}$ is to be defined centering around the direction of each photon in the pseudo-rapidity (η) and azimuthal angle (ϕ) plane. It is then demanded that in order to satisfy the isolation criteria, the sum of the hadronic transverse energy $H(r)$ has to be always less than $H(r)_{\rm max}$ for all cones with radius $r \leq r_0$. In the present analysis, we have taken following choice of $H(r)_{\rm max}$ defined as,

$$H(r)_{\rm max} = \epsilon_\gamma \; E_T^\gamma \left(\frac{1 - \cos r}{1 - \cos r_0} \right)^n \quad , \tag{4}$$

where E_T^γ is the transverse energy of the photon and ϵ_γ, r_0 and n are three FI parameters that are to be specified while applying such isolation.

On-shell Z and $W^\pm$ have been produced while generating events for ZZ and W^+W^- production processes respectively. The two Z bosons are then leptonically decayed to e^+e^- and $\mu^+\mu^-$ respectively at the time of showering. The decay channels $W^+ \to e^+\nu_e$ and $W^- \to \mu^-\bar{\nu}_\mu$ have been taken into account while showering W^+W^- events.

Owing to the tremendous development in computation of NLO correction in the last few years, automation plays an important role throughout this work. The universal FeynRules [26] output (UFO) of the RS model has been imported within the MadGraph5 (MG5) environment [27]. We choose to work in the MG5_aMC@NLO framework [23] in which the Born level square matrix elements are generated using MG5 and calculation of the real emission cross sections together with their singularities are overseen by MadFKS [28] package which uses the FKS subtraction scheme [29] in an automated way. However, a set of external FORTRAN codes, that handle virtual contributions, have been prepared using the analytical results involving one-loop amplitudes for e^+e^- [30], $\gamma\gamma$ [11], ZZ [14], W^+W^- [16] in the SM & RS model and they have been systematically implemented into this framework. Nevertheless, another in-house FORTRAN code which takes care of the summation of KK-tower propagators, has suitably been fitted in this environment, thereby making essential and appropriate changes in the spin-2 HELAS routines [18]. We have explicitly checked numerical cancellation of double and single poles coming from the real and virtual parts for all these processes and thereafter used this complete set-up to generate corresponding events. The generated events are then matched with HERWIG6 [31] parton shower using aMC@NLO, where the MC@NLO formalism is being automatised. Uncertainties in renormalisation (μ_R) and factorisation (μ_F) scale and in parton distribution functions (PDF) are also estimated in an automated way with no extra CPU cost. Note that, instead of decaying a particle at the time of showering, it is also possible to decay it into its preferred decay channel at the event generation level itself by making the use of MadSpin [32] that restrains nearly all spin correlations. However, to use the same for Z or $W^\pm$ decay is beyond the scope of this paper due to the significant complexity involved in including KK-tower summation and changing HELAS [33, 34] routines accordingly.

3 Numerical Results

In this section, we present a number of differential distributions of various kinematical observables at the NLO+PS accuracy for e^+e^-, $\gamma\gamma$, ZZ, W^+W^- production processes at the LHC with center of mass energy $\sqrt{S} = 14$ TeV. Following electroweak input parameters have been used at the time of event generation: (*i*) $\alpha_{EW}^{-1} = 132.507$, (*ii*) $G_F = 1.16639 \times 10^{-5}$ GeV^{-2}, (*iii*) $M_Z = 91.188$ GeV and using them as input the mass of W boson $M_W = 80.419$ GeV and $\sin^2\theta_w = 0.222$

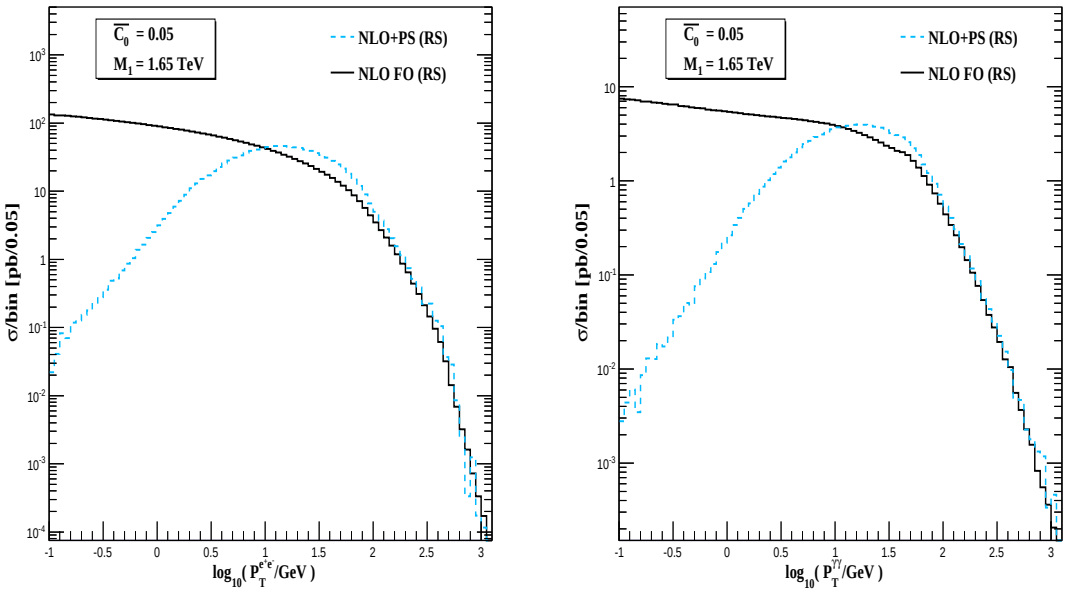

Figure 1: Transverse momentum distribution of RS contribution, shown in log-log scale at fixed order NLO and NLO+PS for the Drell-Yan (left) and di-photon (right) production processes.

are evaluated. We have considered $n_f = 5$ massless quark flavors in our present study. The central choices of μ_R and μ_F are always set equal to the invariant mass of the corresponding di-final state. MSTW(n)lo2008cl68 PDF sets [35] have been used throughout the analysis in order to generate (N)LO events and they determine the value of strong coupling α_s. (N)LO events are generated with very loose cuts on transverse momentum (P_T) and rapidity (y) of the final state particles and they are detailed here under: (a) Drell-Yan: $P_T^{e^+,e^-} \geq 15$ GeV, $|y^{e^+,e^-}| \leq 2.7$, $\Delta R^{e^+e^-} > 0.3$, where $\Delta R = \sqrt{(\Delta y)^2 + (\Delta\phi)^2}$ denotes the separation between two particles in the rapidity-azimuthal angle plane, (b) Di-photon: $P_T^{\gamma} \geq 15$ GeV, $|y^{\gamma}| \leq 2.7$ with a set of particular FI parameters *i.e.*, $\epsilon_\gamma = 1$, $r_0 = 0.3$ and $n = 2$. However, no such kinematical cuts have been provided while generating events for ZZ and W^+W^- processes. Besides, for W^+W^- event generation we have taken diagonal unit CKM matrix and neglected top quark contribution in the whole analysis.

The events thus generated are then matched with HERWIG6 [31] parton shower Monte Carlo using the MC@NLO formalism [24]. While showering di-lepton events, $P_T^l \geq 20$ GeV, $|y^l| \leq 2.5$, $\Delta R^{ll} > 0.4$ have been used for the analysis purpose, where $l = e^+, e^-$. In order to separate leptons from jets $\Delta R^{lj} > 0.7$ has also been applied at this stage and finally we have found out hardest e^+ and e^- to build several kinematical observables with them. In case of showering di-photon events, following analysis cuts are put on each photon with the following FI parameters: $P_T^{\gamma} \geq 20$ GeV, $|y^{\gamma}| \leq 2.5$, $\Delta R^{\gamma\gamma} > 0.4$ and $\epsilon_\gamma = 1$, $r_0 = 0.4$, $n = 2$ and we have collected

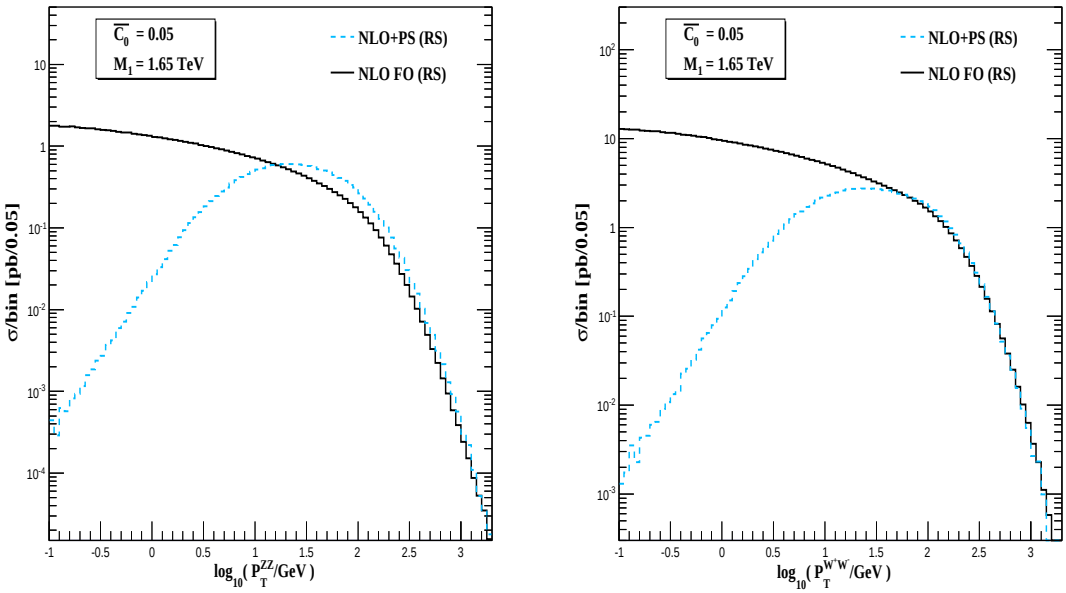

Figure 2: Transverse momentum distribution of RS contribution, shown in log-log scale at fixed order NLO and NLO+PS for the ZZ (left) and W^+W^- (right) production processes.

two hardest photons γ_1, γ_2 among many others. As described earlier, Z bosons are leptonically decayed at the time of showering ZZ events and the applied analysis cuts are as follows: $P_T^l \geq 20$ GeV, $|y^l| \leq 2.5$, $\Delta R^{ll} > 0.4$, $\Delta R^{lj} > 0.7$, where $l = e^+, e^-, \mu^+, \mu^-$. After that, all the final state stable leptons (*i.e.*, $e^\pm, \mu^\pm$) are being collected to make pair of leptons that have equal flavor but opposite charge. Finally we have selected those leptons that are contributing as the hardest e^+e^- and $\mu^+\mu^-$ pairs with the condition that their invariant masses ($M^{l^+l^-}$) satisfy the criteria $|M^{l^+l^-} - M_Z| < 10$ GeV, to make sure that those leptons are actually decay products of the Z bosons. At the time of showering W^+W^- events with their corresponding decay modes, we have identified the final state stable lepton-neutrino pair whose mother is one of the $W^\pm$ bosons and make them pass through the following set of analysis cuts: $P_T^l \geq 20$ GeV, $|y^l| \leq 2.5$, $\Delta R^{ll} > 0.4$, $\Delta R^{lj} > 0.7$ and $\not{E}_T > 30$ GeV. We have checked that all the above events generated in each processes produce completely unbiased results with the appliance of our present choices of generation and analysis cuts.

To show the effect of parton shower over the fixed order NLO results, we have presented in Fig. (1) the $\log_{10} P_T$ distributions of the e^+e^- (left) and $\gamma\gamma$ (right) pair at fixed order NLO (solid black) as well as in NLO+PS (dashed blue) accuracy for the RS case. Both the curves in each figure are plotted using respective analysis cuts and we have used the RS model parameter $\overline{c_0} = 0.05$ and the corresponding M_1 value is taken as $M_1 = 1.65$ TeV. Note that, by the label 'RS' in the figure, we

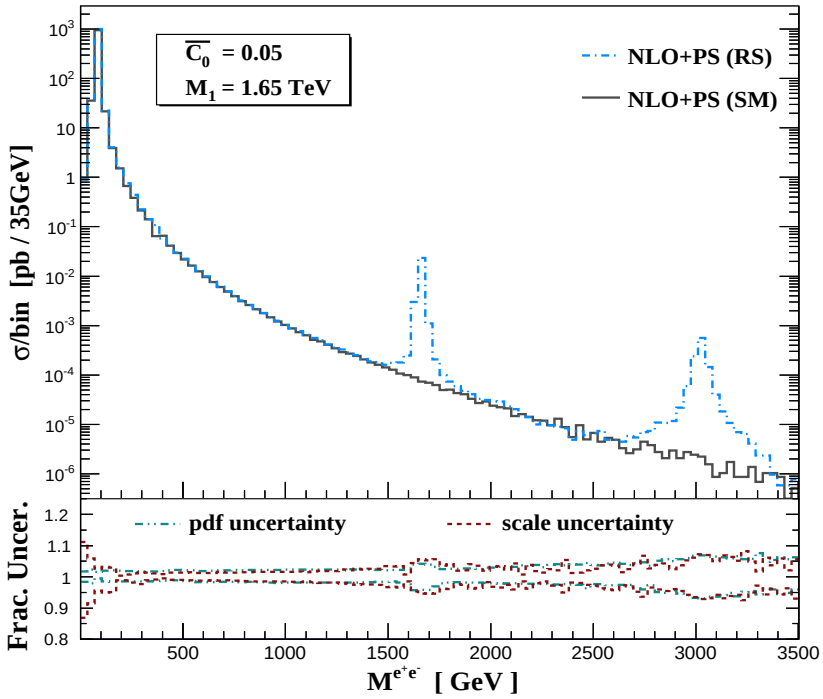

Figure 3: Invariant mass distribution of the di-lepton pair in Drell-Yan process for RS and SM.

mean the total contribution that consists of SM, RS and the interference between the two and we maintain the same convention in the rest of the figures as well. Likewise, Fig. (2) represents similar distributions for the ZZ (left) and W^+W^- (right) pairs. Each of these figures shows diverging nature of the fixed order NLO curve in the $P_T \to 0$ region, whereas the NLO+PS result gets convergent in that region ensuring the correct resummation of the Sudakov logarithms and thereby leading to a suppression in cross section in the low-P_T region. As expected, both the results are in good agreement with one another in the high-P_T region.

Uncertainty calculations of various distributions have been performed automatically in the aMC@NLO framework by using its built-in re-weighting procedure that stores sufficient information in the parton level Les Houches event files. Independent variation of μ_R and μ_F scales are considered to calculate scale uncertainties. We have set $\mu_R = \xi_R M$ and $\mu_F = \xi_F M$, where M denotes the invariant mass of the di-final state (*i.e.*, $M^{e^+e^-}$, $M^{\gamma\gamma}$, M^{ZZ} or $M^{W^+W^-}$, as applicable) and ξ_R, ξ_F can take any one of the values $(1, 1/2, 2)$ at a time. The scale uncertainty band would then be determined as the envelope [18] of the following (ξ_R, ξ_F) combinations: $(1, 1)$, $(1, 1/2)$, $(1, 2)$, $(1/2, 1/2)$, $(1/2, 1)$, $(2, 1)$, $(2, 2)$. On the other hand, PDF uncertainties are estimated using Hessian method as prescribed by the MSTW collaboration [35].

In all the subsequent figures, various distributions of kinematical observables

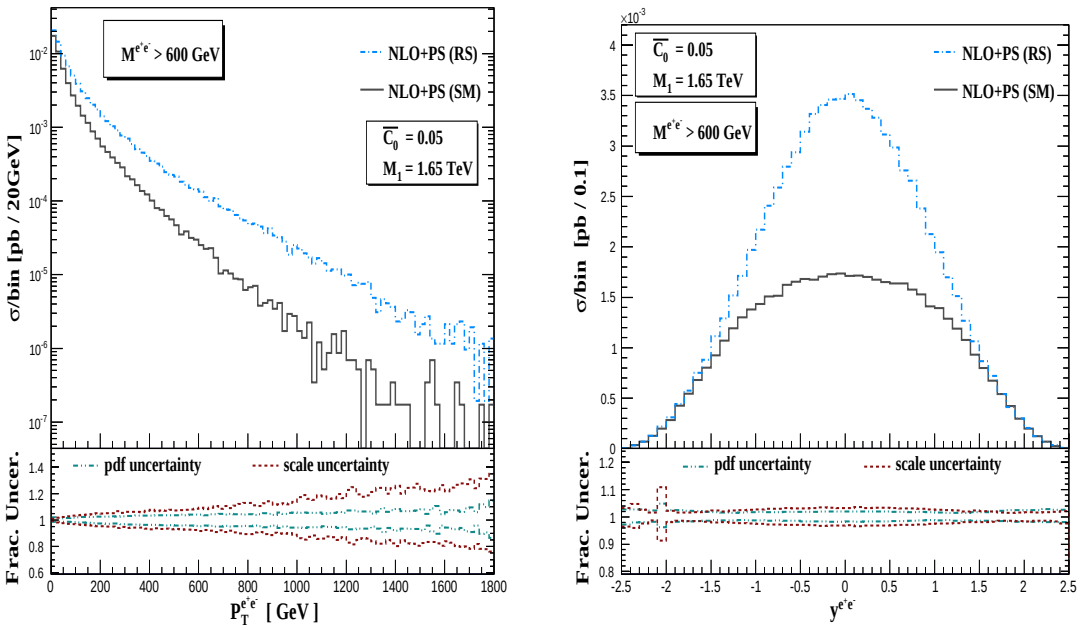

Figure 4: Transverse momentum (left) and rapidity (right) distribution of the dilepton pair in both RS and SM.

are depicted using a consistent graphical representation. In the Figures the main frame, depicts distributions that are of outcome of both the RS (dash-dotted blue) and SM (solid black), are shown to NLO+PS accuracy, whereas the corresponding lower insets provide the estimation of the fractional scale (dashed red) and PDF (dash-double dotted green) uncertainties, which basically denote the variation of the central value (*i.e*, the extremum value divided by the central value). Unless stated otherwise, $\overline{c_0} = 0.05$ and $M_1 = 1.65$ TeV are used in all these plots.

For the Drell-Yan production process, invariant mass distribution of the e^+e^- pair is shown in Fig. (3). The two peaks in the RS case indicate first (M_1) and second (M_2) excitations of the RS graviton and they perfectly match with the theoretical values (see Eq. 3). Fig. (4), (5) and (6) apprise the transverse momentum (left) and rapidity (right) distributions of the e^+e^- pair, e^+ and e^- respectively in the region $M^{e^+e^-} > 600$ GeV. Such invariant mass cut, which is also applied consistently to the rest processes, is an optimal choice to reduce SM background effects, ensuring the influence of sufficient signal events at the same time. Individually, transverse momentum distributions of e^+ and e^- are of similar kind and two kinks are arising near the half of the M_1 and M_2 values. However, in the combined transverse momentum distribution of the e^+e^- pair, washing out of such kinks points out that the directions of outgoing e^+ and e^- are opposite to each other in the transverse plane of the beam direction. The fractional uncertainties associated with these P_T distributions are large in the high transverse momentum region, although they are

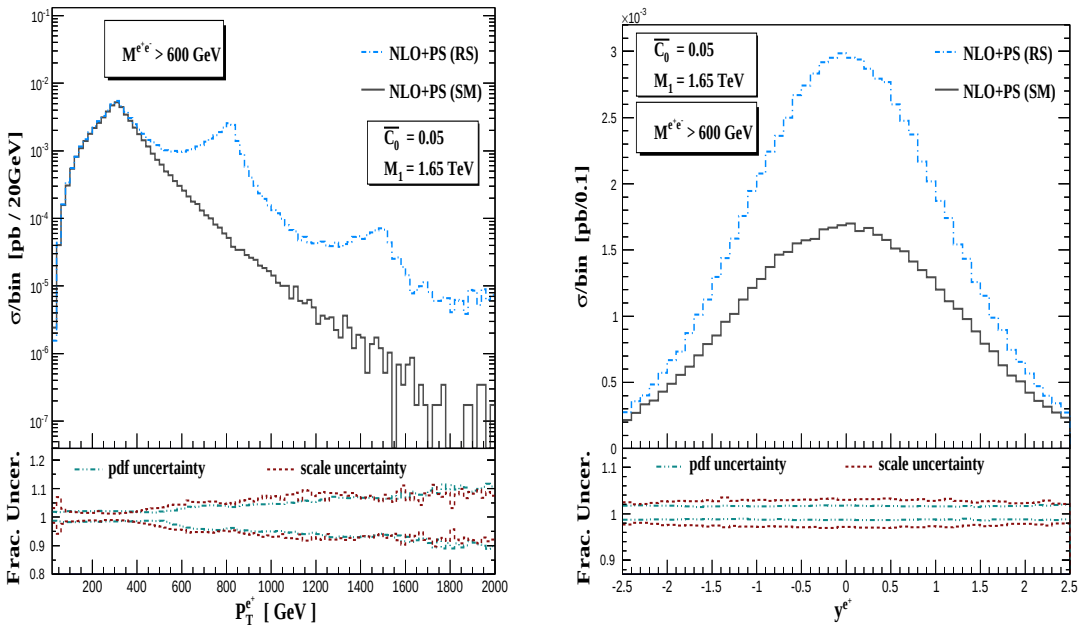

Figure 5: Transverse momentum (left) and rapidity (right) distribution of the positron for the Drell-Yan production process in SM and RS.

quite minimal in the low-P_T region, where the higher order effects are included as a result of resummation. In the high-P_T region of e^+e^- pair, the large uncertainty is a reflection of the fact that it is in fact a leading order process. Note that, the rapidity distributions of e^+ and e^- are not similar because the high invariant mass cut is responsible in breaking the angular correlation between them. To estimate the improvement in the results while including NLO corrections, we find that the scale uncertainties in the central rapidity region of all these rapidity distributions in the RS case reduce to about 6-8% in NLO+PS, from about 10-12% at LO+PS. PDF uncertainties in NLO+PS are about 1-1.5% less compared to the LO+PS outcomes.

Distributions related to the di-photon production are shown in Fig. (7)-(9). In Fig. (7), we have presented invariant mass (left) distribution of the diphoton system and the separation (right) between the two hardest photons in the rapidity-azimuthal angle plane with the cut $M^{\gamma\gamma} > 600$ GeV. The invariant mass distribution clearly shows two peaks that correspond to the choice of M_1 value and the respective M_2 value derived from that. The $\Delta R^{\gamma\gamma}$ distributions are almost same for SM and RS and the peaks near the angle π (*i.e.*, 180°) in these distributions indicate the abundance of such two hardest photons that are mostly back-to-back and the associated scale uncertainty is becoming almost nil as the two photons are getting much away from one another. Fig. (8) and (9) represent the transverse momentum (left) and rapidity (right) distributions of the di-photon system and the hardest photon respectively in

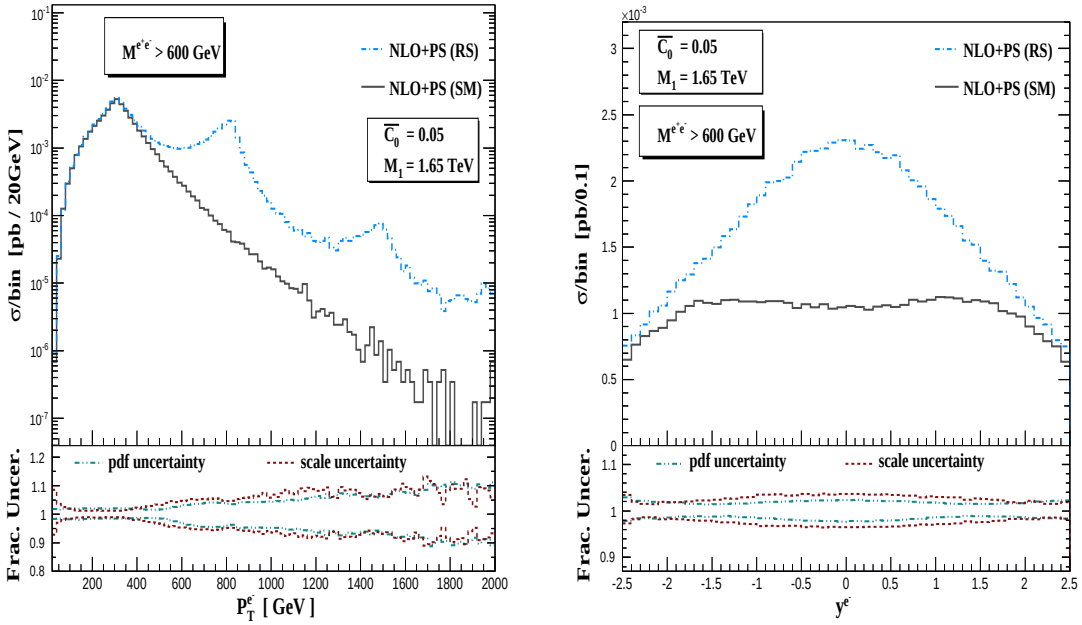

Figure 6: Transverse momentum (left) and rapidity (right) distribution of the electron for the Drell-Yan production process in SM and RS.

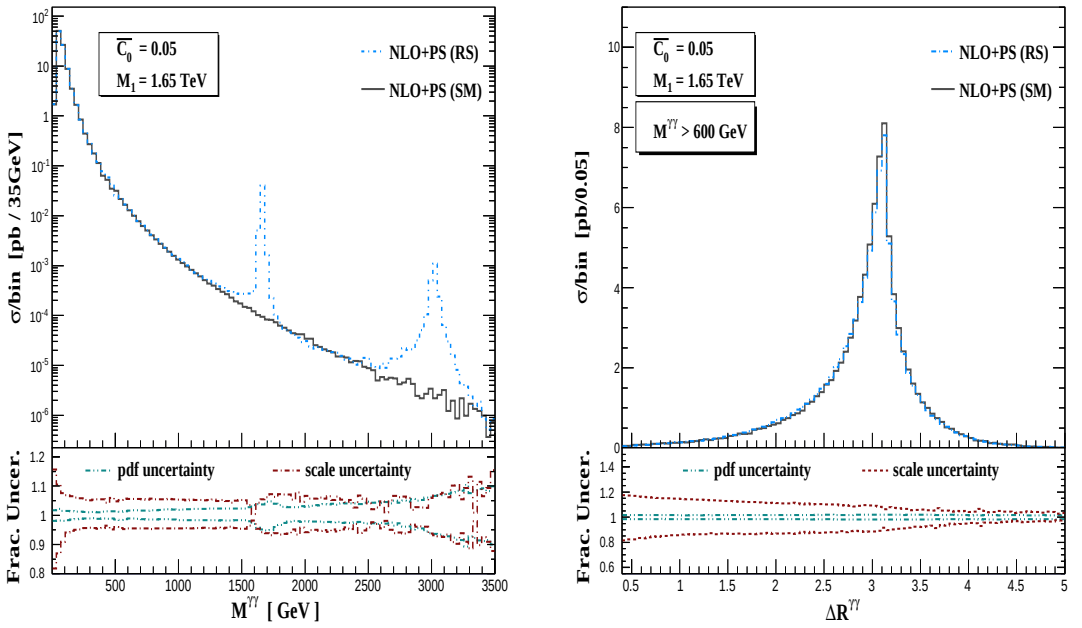

Figure 7: Invariant mass distribution of the di-photon pair (left) in RS and SM. The right panel shows the separation between two hardest photons in the rapidity-azimuthal angle plane.

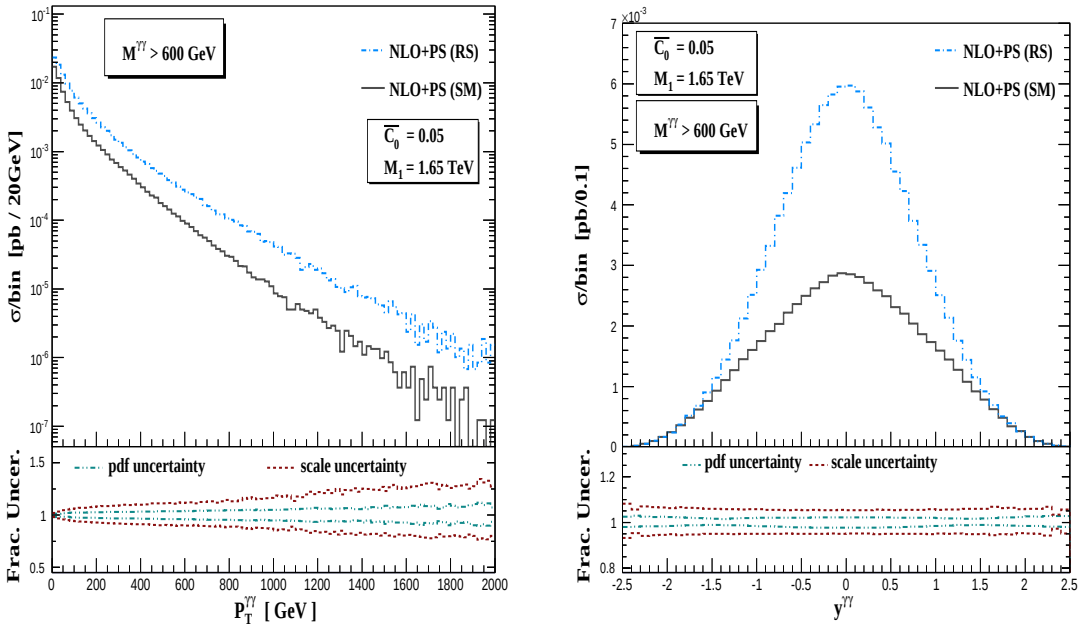

Figure 8: Di-photon transverse momentum (left) and rapidity (right) distribution in RS and SM.

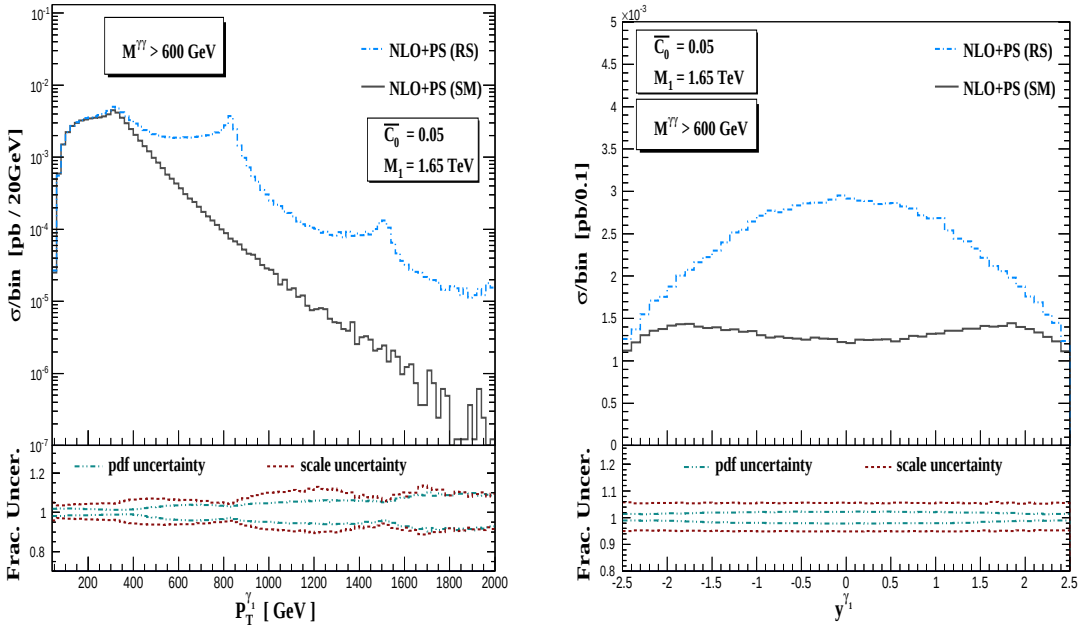

Figure 9: Transverse momentum (left) and rapidity (right) distribution of the hardest photon in di-photon production process in RS and SM.

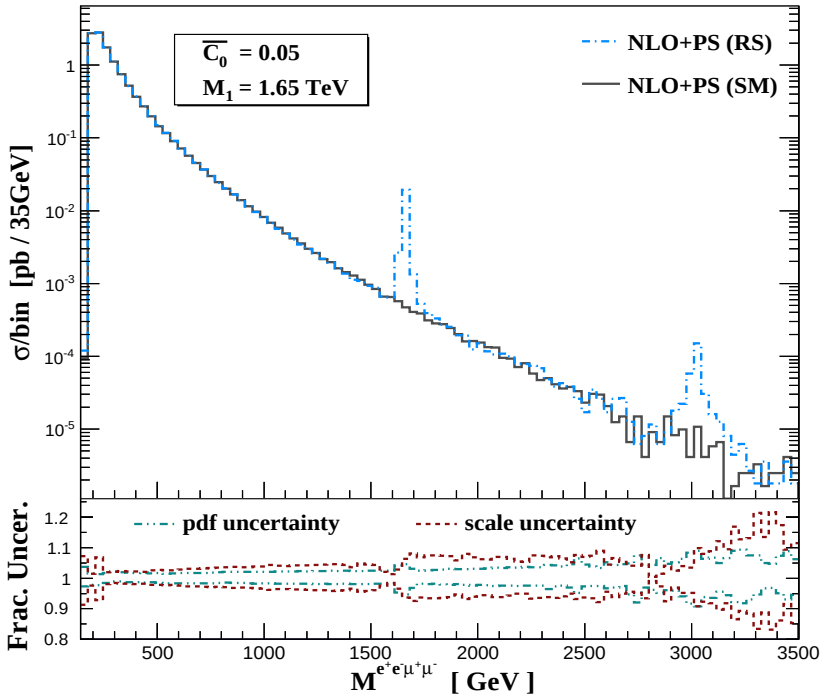

Figure 10: Four-lepton invariant mass ($M^{e^+e^-\mu^+\mu^-}$) distribution for RS and SM coming from the decay products of ZZ process.

the region where the condition $M^{\gamma\gamma} > 600$ GeV is satisfied. Here also, we are getting two kinks in the transverse momentum distribution of the individual hardest photon around the half of the first and second excitation values of the RS graviton. The scale uncertainties in the central rapidity regions in LO+PS were around 13-14% and they are as expected reduced to 10% in NLO+PS, although the reduction in PDF uncertainties is only about 0.2% between the NLO+PS and LO+PS results.

Fig. (10)-(12) correspond to the distributions of decay products that are coming from the ZZ events. The invariant mass ($M^{e^+e^-\mu^+\mu^-}$) distribution of all the final state leptons is depicted in Fig. (10). As expected, there are two peaks in this distribution indicating the first two excitations of the graviton considered in the RS model. The transverse momentum (left) and rapidity (right) distributions of the e^+e^- pair and $\mu^+\mu^-$ pair are respectively shown in Fig. (11) and (12) with the insertion of $M^{e^+e^-\mu^+\mu^-} > 600$ GeV cut. In these P_T distributions the first kink is visible at the half value of the first excitation. The rapidity distributions of those pairs are not alike because of the same reason of applying aforesaid high invariant mass cut for which the angular correlation between the decay products of the two Z bosons has been lost.

Few selective distributions that are coming from W^+W^- events are given in Fig. (13) and (14). The left panel of Fig. (13) shows the invariant mass ($M^{e^+\mu^-\not{E}_T}$) distribution of the $W^\pm$ decay products and in the right panel of this figure, we have

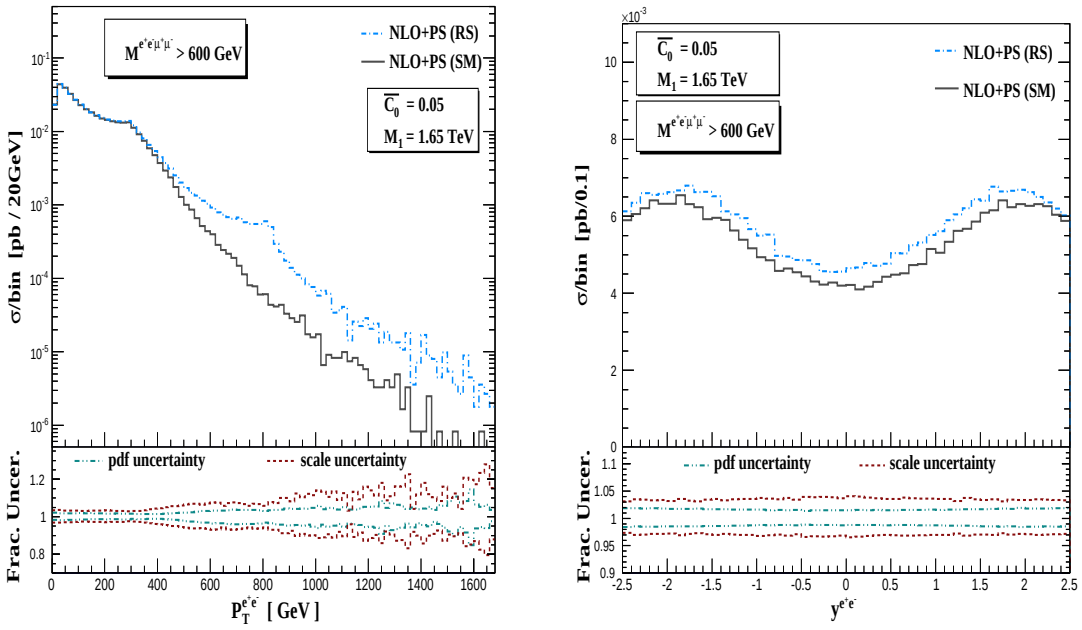

Figure 11: Transverse momentum (left) and rapidity (right) distribution of the e^+e^- pair coming from the decay products of ZZ process in RS and SM.

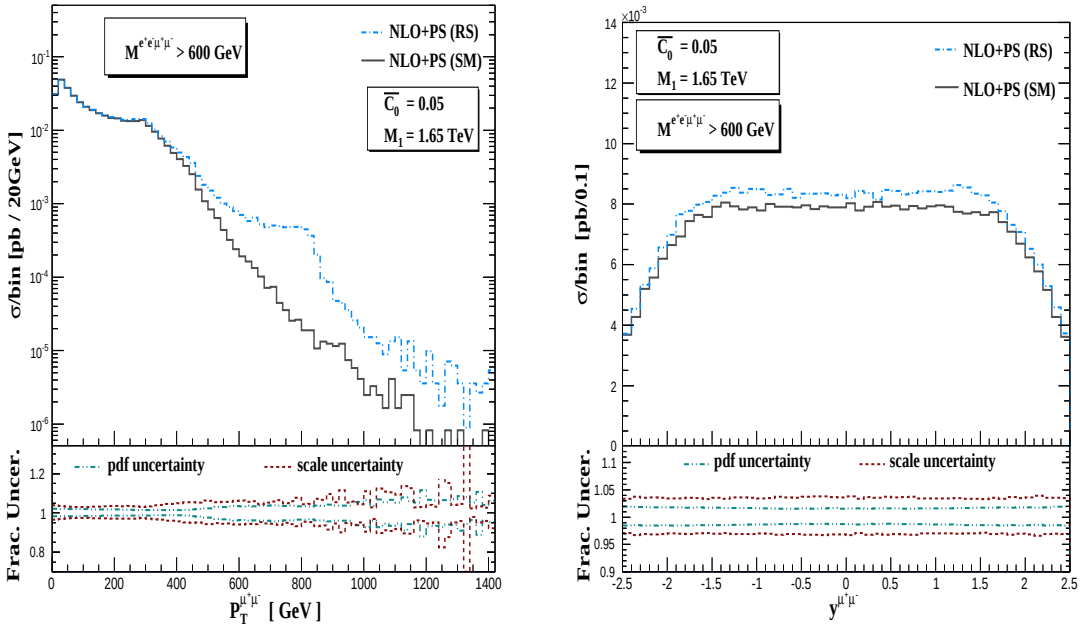

Figure 12: Transverse momentum (left) and rapidity (right) distribution of the $\mu^+\mu^-$ pair coming from ZZ decay for RS and SM.

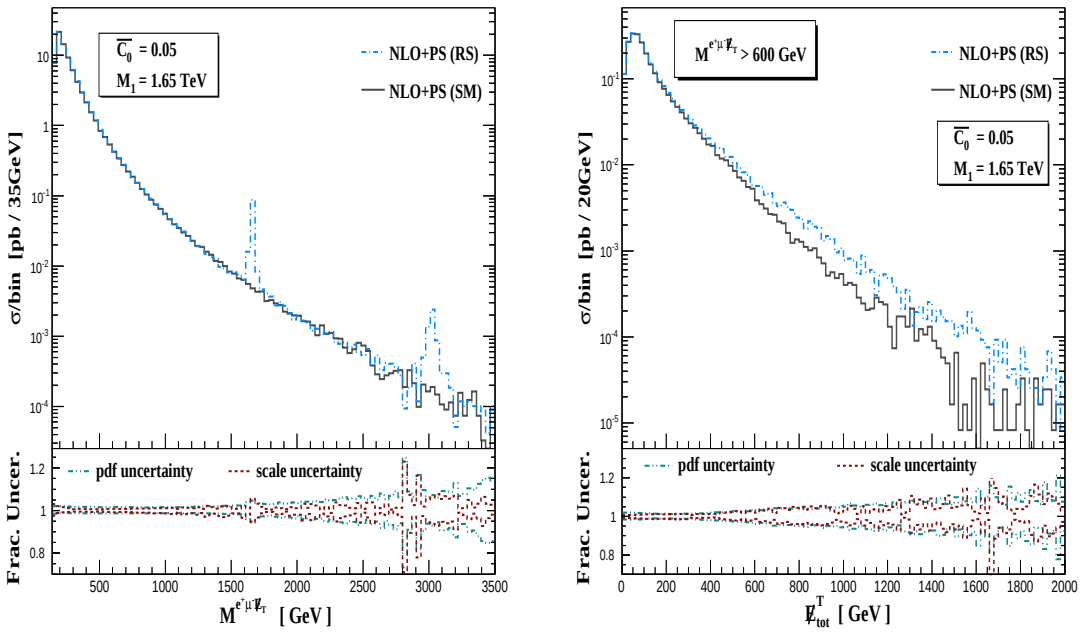

Figure 13: Invariant mass (left) distribution of the decay products of $W^{\pm}$ and the total missing $\not{E}_T$ distribution (right) in SM and RS.

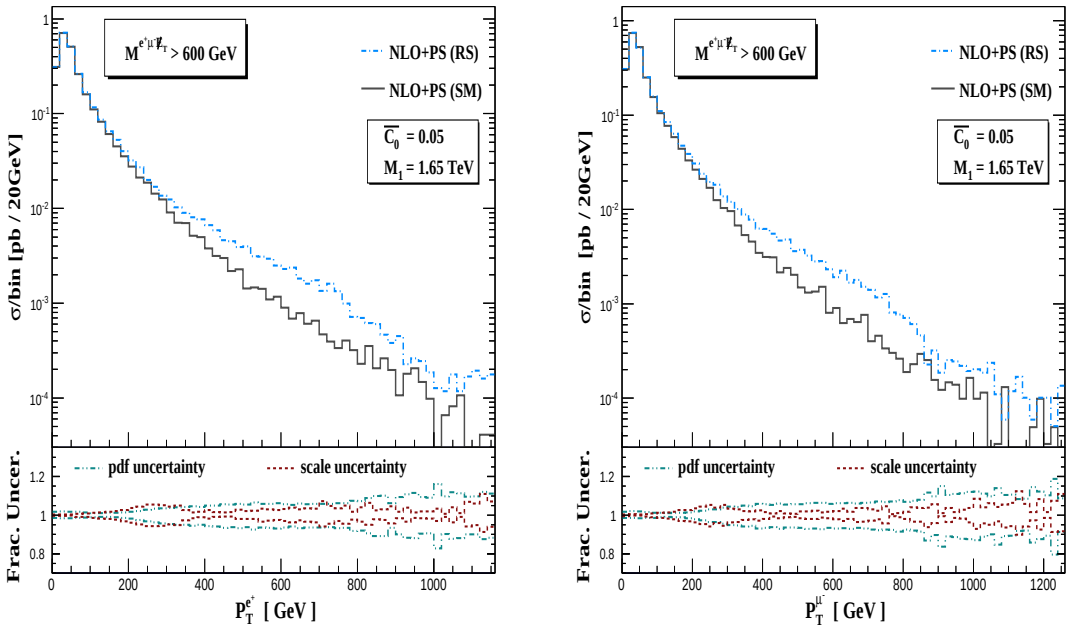

Figure 14: Transverse momentum distribution of e^+ (left) and μ^- (right) coming from $W^{\pm}$ decay in RS and SM.

presented the transverse missing energy ($\not{E}_T$) distribution that is coming from the electron neutrino and muon anti-neutrino which practically escape the experimental detection in the collider. $M^{e^+\mu^-\not{E}_T} > 600$ GeV cut is used for the later one to differentiate the missing $\not{E}_T$ signal of the RS from the SM one. In Fig. (14), the transverse momentum distributions of the positron (left) and the muon (right) are shown in the region where $M^{e^+\mu^-\not{E}_T} > 600$ GeV and we find that the distribution in the RS case is comparatively harder than the SM distribution in this region.

$\bar{c}_0$	0.03	0.05	0.07	0.10
$M_1^{(3\sigma)}$ (TeV)	4.5	6.3	7.4	10.3
$M_1^{(5\sigma)}$ (TeV)	4.2	5.2	6.0	8.3

Table 1: Bounds on M_1 for various $\bar{c}_0$ values at the 14 TeV LHC with integrated luminosity of 50 fb^{-1} at 3-sigma and 5-sigma signal significance, coming from Drell-Yan process.

Here, we investigate the search sensitivity of the RS model using the Drell-Yan and di-photon processes for the following $\overline{c}_0$ values at the 14 TeV LHC: $\overline{c}_0 = 0.03, 0.05, 0.07, 0.10$. We have calculated the total cross section for the signal plus background and the background alone using the invariant mass distribution of the e^+e^- ($\gamma\gamma$) pair in Drell-Yan (di-photon) production and estimated the minimum required luminosity that distinguishes the signal from the background at 3-sigma (3σ) and 5-sigma (5σ) signal significance for various values of M_1 for a fixed $\overline{c}_0$. The required minimum luminosity is defined as, $L_{\rm min} = \max\{L_{3\sigma(5\sigma)}, L_{3N_S(5N_S)}\}$, where $L_{3\sigma(5\sigma)}$ describes the integrated luminosity at 3-sigma (5-sigma) signal significance and $L_{3N_S(5N_S)}$ denotes the integrated luminosity to have at least 3(5) signal events. From the data set of M_1 *vs.* $L_{\rm min}$ thus prepared, by inversion we find the M_1 value that corresponds to 50 fb^{-1} luminosity for each of the $\overline{c}_0$ values listed above and those bounds that are counted using Drell-Yan and di-photon processes are tabulated in Table 1 and 2 respectively. Of course, a full analysis including the effects of detector simulation, non-reducible backgrounds etc. would lead these bounds to their betterment.

$\bar{c}_0$	0.03	0.05	0.07	0.10
$M_1^{(3\sigma)}$ (TeV)	5.2	5.6	6.1	7.5
$M_1^{(5\sigma)}$ (TeV)	5.0	5.3	5.6	6.4

Table 2: Bounds on M_1 for various $\bar{c}_0$ values at the 14 TeV LHC with integrated luminosity of 50 fb^{-1} at 3-sigma and 5-sigma signal significance, coming from di-photon production process.

4 Conclusions

In this paper, we have studied all the important di-final state processes ($\ell^+\ell^-$, $\gamma\gamma$, ZZ and W^+W^-) in the RS model to NLO+PS accuracy, implemented in the aMC@NLO framework. All the subprocesses to NLO in QCD have been taken into account for both the SM and RS model. For the di-final state processes under consideration, we demonstrate the importance of NLO+PS results over the fixed order NLO computations, by studying the p_T distribution of the di-final states. For suitable choice of RS model parameters, a selection of the results for various observables at the 14 TeV LHC are presented. PDF and scale uncertainties are presented for the various distributions which significantly reduce with the inclusion of NLO corrections. The di-lepton and di-photon processes are used to study the search sensitivity of the RS model at 14 TeV LHC with 50 fb^{-1} luminosity. The stand-alone codes can be used to generate events with any choice of RS model parameters for di-final state processes discussed in this paper to NLO+PS accuracy and are being made available on the website `http://amcatnlo.cern.ch`.

Acknowledgements

We would like to acknowledge the High Performance Computing facility of Theory Division, SINP where the computational work has been carried out. GD would like to thank Paolo Torrielli, Marco Zaro and M. C. Kumar for important suggestions.

References

[1] N. Arkani-Hamed, S. Dimopoulos, and G. Dvali, *The Hierarchy problem and new dimensions at a millimeter*, *Phys.Lett.* **B429** (1998) 263–272, [hep-ph/9803315].

[2] I. Antoniadis, N. Arkani-Hamed, S. Dimopoulos, and G. Dvali, *New dimensions at a millimeter to a Fermi and superstrings at a TeV*, *Phys.Lett.* **B436** (1998) 257–263, [hep-ph/9804398].

[3] L. Randall and R. Sundrum, *A Large mass hierarchy from a small extra dimension*, *Phys.Rev.Lett.* **83** (1999) 3370–3373, [hep-ph/9905221].

[4] H. Davoudiasl, J. Hewett, and T. Rizzo, *Phenomenology of the Randall-Sundrum Gauge Hierarchy Model*, *Phys.Rev.Lett.* **84** (2000) 2080, [hep-ph/9909255].

[5] **CMS Collaboration** Collaboration, S. Chatrchyan et al., *Search for Resonances in the Dilepton Mass Distribution in pp Collisions at* $\sqrt{(}s) = 7$ *TeV*, *JHEP* **1105** (2011) 093, [arXiv:1103.0981].

[6] **CMS Collaboration** Collaboration, S. Chatrchyan et al., *Search for signatures of extra dimensions in the diphoton mass spectrum at the Large Hadron Collider*, *Phys.Rev.Lett.* **108** (2012) 111801, [arXiv:1112.0688].

[7] **ATLAS Collaboration** Collaboration, G. Aad et al., *Search for Extra Dimensions using diphoton events in 7 TeV proton-proton collisions with the ATLAS detector*, *Phys.Lett.* **B710** (2012) 538–556, [arXiv:1112.2194].

[8] **ATLAS Collaboration** Collaboration, G. Aad et al., *Search for Extra Dimensions in diphoton events using proton-proton collisions recorded at $\sqrt{s} = 7$ TeV with the ATLAS detector at the LHC*, *New J.Phys.* **15** (2013) 043007, [arXiv:1210.8389].

[9] P. Mathews, V. Ravindran, K. Sridhar, and W. van Neerven, *Next-to-leading order QCD corrections to the Drell-Yan cross section in models of TeV-scale gravity*, *Nucl.Phys.* **B713** (2005) 333–377, [hep-ph/0411018].

[10] M. Kumar, P. Mathews, and V. Ravindran, *PDF and scale uncertainties of various DY distributions in ADD and RS models at hadron colliders*, *Eur.Phys.J.* **C49** (2007) 599–611, [hep-ph/0604135].

[11] M. Kumar, P. Mathews, V. Ravindran, and A. Tripathi, *Direct photon pair production at the LHC to order α_s in TeV scale gravity models*, *Nucl.Phys.* **B818** (2009) 28–51, [arXiv:0902.4894].

[12] M. Kumar, P. Mathews, V. Ravindran, and A. Tripathi, *Diphoton signals in theories with large extra dimensions to NLO QCD at hadron colliders*, *Phys.Lett.* **B672** (2009) 45–50, [arXiv:0811.1670].

[13] N. Agarwal, V. Ravindran, V. Tiwari, and A. Tripathi, *Z boson pair production at the LHC to O(alpha(s)) in TeV scale gravity models*, *Nucl.Phys.* **B830** (2010) 248–270, [arXiv:0909.2651].

[14] N. Agarwal, V. Ravindran, V. K. Tiwari, and A. Tripathi, *Next-to-leading order QCD corrections to the Z boson pair production at the LHC in Randall Sundrum model*, *Phys.Lett.* **B686** (2010) 244–248, [arXiv:0910.1551].

[15] N. Agarwal, V. Ravindran, V. K. Tiwari, and A. Tripathi, *W^+W^- production in Large extra dimension model at next-to-leading order in QCD at the LHC*, *Phys.Rev.* **D82** (2010) 036001, [arXiv:1003.5450].

[16] N. Agarwal, V. Ravindran, V. K. Tiwari, and A. Tripathi, *Next-to-leading order QCD corrections to W^+W^- production at the LHC in Randall Sundrum model*, *Phys.Lett.* **B690** (2010) 390–395, [arXiv:1003.5445].

[17] S. A. Li, C. S. Li, H. T. Li, and J. Gao, *Constraints on Randall-Sundrum model from the events of dijet production with QCD next-to-leading order accuracy at the LHC*, arXiv:1408.2762.

[18] R. Frederix, M. K. Mandal, P. Mathews, V. Ravindran, S. Seth, et al., *Diphoton production in the ADD model to NLO+parton shower accuracy at the LHC*, *JHEP* **1212** (2012) 102, [arXiv:1209.6527].

[19] R. Frederix, M. Mandal, P. Mathews, V. Ravindran, and S. Seth, *Drell-Yan, ZZ, W^+W^- production in SM & ADD model to NLO+PS accuracy at the LHC*, *Eur.Phys.J.* **C74** (2014) 2745, [arXiv:1307.7013].

[20] D. de Florian, M. Mahakhud, P. Mathews, J. Mazzitelli, and V. Ravindran, *Quark and gluon spin-2 form factors to two-loops in QCD*, *JHEP* **1402** (2014) 035, [arXiv:1312.6528].

[21] D. de Florian, M. Mahakhud, P. Mathews, J. Mazzitelli, and V. Ravindran, *Next-to-Next-to-Leading Order QCD Corrections in Models of TeV-Scale Gravity*, *JHEP* **1404** (2014) 028, [arXiv:1312.7173].

[22] T. Ahmed, M. Mahakhud, P. Mathews, N. Rana, and V. Ravindran, *Two-Loop QCD Correction to massive spin-2 resonance $\to$ 3 gluons*, *JHEP* **1405** (2014) 107, [arXiv:1404.0028].

[23] J. Alwall, R. Frederix, S. Frixione, V. Hirschi, F. Maltoni, et al., *The automated computation of tree-level and next-to-leading order differential cross sections, and their matching to parton shower simulations*, *JHEP* **1407** (2014) 079, [arXiv:1405.0301].

[24] S. Frixione and B. R. Webber, *Matching NLO QCD computations and parton shower simulations*, *JHEP* **0206** (2002) 029, [hep-ph/0204244].

[25] S. Frixione, *Isolated photons in perturbative QCD*, *Phys.Lett.* **B429** (1998) 369–374, [hep-ph/9801442].

[26] A. Alloul, N. D. Christensen, C. Degrande, C. Duhr, and B. Fuks, *FeynRules 2.0 - A complete toolbox for tree-level phenomenology*, *Comput.Phys.Commun.* **185** (2014) 2250–2300, [arXiv:1310.1921].

[27] J. Alwall, M. Herquet, F. Maltoni, O. Mattelaer, and T. Stelzer, *MadGraph 5 : Going Beyond*, *JHEP* **1106** (2011) 128, [arXiv:1106.0522].

[28] R. Frederix, S. Frixione, F. Maltoni, and T. Stelzer, *Automation of next-to-leading order computations in QCD: The FKS subtraction*, *JHEP* **0910** (2009) 003, [arXiv:0908.4272].

[29] S. Frixione, Z. Kunszt, and A. Signer, *Three jet cross-sections to next-to-leading order*, *Nucl.Phys.* **B467** (1996) 399–442, [hep-ph/9512328].

[30] P. Mathews, V. Ravindran, and K. Sridhar, *NLO-QCD corrections to dilepton production in the Randall-Sundrum model*, *JHEP* **0510** (2005) 031, [hep-ph/0506158].

[31] G. Corcella, I. Knowles, G. Marchesini, S. Moretti, K. Odagiri, et al., *HERWIG 6: An Event generator for hadron emission reactions with interfering gluons (including supersymmetric processes)*, *JHEP* **0101** (2001) 010, [hep-ph/0011363].

[32] P. Artoisenet, R. Frederix, O. Mattelaer, and R. Rietkerk, *Automatic spin-entangled decays of heavy resonances in Monte Carlo simulations*, *JHEP* **1303** (2013) 015, [arXiv:1212.3460].

[33] H. Murayama, I. Watanabe, and K. Hagiwara, *HELAS: HELicity amplitude subroutines for Feynman diagram evaluations*, *KEK-91-11* (1992).

[34] P. de Aquino, K. Hagiwara, Q. Li, and F. Maltoni, *Simulating graviton production at hadron colliders*, *JHEP* **1106** (2011) 132, [arXiv:1101.5499].

[35] A. Martin, W. Stirling, R. Thorne, and G. Watt, *Parton distributions for the LHC*, *Eur.Phys.J.* **C63** (2009) 189–285, [arXiv:0901.0002].